

# Super-Trajectory for Video Segmentation

Wenguan Wang, and Jianbing Shen, *Senior Member, IEEE*

**Abstract**—We propose a semi-supervised video segmentation via an efficient video representation, called as “super-trajectory”. Each super-trajectory corresponds to a group of compact trajectories that exhibit consistent motion patterns, similar appearance and close spatiotemporal relationships. To handle occlusions and drifts, we develop a trajectory generation method based on probabilistic model, which is more reasonable and interpretable than traditional trajectory methods using hard thresholding. We then modify a density peaks based clustering algorithm for reliably grouping trajectories, thus capturing a rich set of spatial and temporal relations among trajectories. Via this discriminative video representation, manual effort on the first frame can be efficiently propagated into the rest of frames. Experimental results on challenging benchmark demonstrate the proposed approach is capable of distinguishing object from complex background and even re-identifying object with long-term occlusions.

## I. INTRODUCTION

In this paper, we address the problem of semi-supervised video segmentation, which refers to segmenting objects in video sequences with available annotations on the first frame. Aiming for this task, we describe an efficient video representation, *super-trajectory*, for capturing rich spatiotemporal structure information carried by realistic videos. Each super-trajectory corresponds to a group of trajectories that have compact relations and similar natures. Such representation captures a rich set of video information:

- *Long term motion information* is effectively exploited by trajectories via tracking points over long periods;
- *Spatial and temporal location information* is explicitly interpreted via clustering spatially and temporally adjacent trajectories; and
- *Compact features*, such as color, motion pattern, are presented via a convenient primitive form of videos.

Super-trajectory captures spatiotemporal structure information as well as greatly reduces the difficulty and complexity of propagating human labels in segmentation. Point trajectory is the block of super-trajectory. For this, we develop a trajectory generation method based on a probabilistic model which handles occlusions and drifts efficiently. Additionally, we modify a density peaks based clustering (DPC) algorithm [1] for obtaining reasonable division of a group of trajectories, thus offering a proper split of videos in time axis. The following two aspects motivate us adopting new trajectory generation strategy and DPC algorithm.

Firstly, for the task of video segmentation, it is desirable to have a powerful video representation that offers a clean



Fig. 1. The proposed super-trajectory based video segmentation takes the first frame as initialization (left column). Benefiting from advantages of super-trajectory, our algorithm achieves promising results even for challenging scenarios such as heavy occlusion, complex appearance distribution, and large shape deformation.

abstract of videos, as well as well handles structure variations and deformations in time and space. Recently released DAVIS dataset [2] presents many challenges typically faced in video object segmentation, such as occlusions, motion blur and appearance changes, while most existing approaches exhibit severe limitations in those cases. That suggests a more explicit video representation is desired and such representation should have some well properties that capture above instances (see Fig. 1).

Secondly, from the perspective of feature generation, traditional trajectory methods are desired to be improved for meeting above requests. Classical point trajectory methods [3], [4], [5], [6] generate trajectories via artificially designed hard-threshold, which easily destroys temporally consistent motion structure, or fails to capture structure variations due to over-precautionary strategy. The proposed trajectory tracking approach is based on a probabilistic model which handles temporal discontinuity interpretably and reasonably. Splitting video sequence (or trajectories) into proper temporal components is essential for handling occlusions. However, it is well-known that, classical clustering methods, such as k-means and spectral clustering, even cannot reached a consensus on the definition of a cluster. We introduce and modify DPC algorithm for grouping trajectories, favoring its good property of choosing cluster centers via a reasonable criterion.

This paper makes the following contributions:

- We propose a novel video segmentation approach based on super-trajectory, which is an explicit representation of video. Such presentation captures spatiotemporal structure information carried by realistic videos via exploring relations among trajectories.
- We present a novel trajectory generation approach based

W. Wang and J. Shen are with Beijing Laboratory of Intelligent Information Technology, School of Computer Science, Beijing Institute of Technology, Beijing 100081, P. R. China. (email: shenjianbing@bit.edu.cn)

on an interpretable probabilistic model, which naturally operates occlusions, drifts and shot boundaries well.

- We introduce a DPC algorithm for efficiently clustering trajectories, which is capable of reliably determining clusters centers and capturing spatiotemporal structure variations.

## II. RELATED WORK

In this section, we provide a brief overview of recent works in video object segmentation and point trajectory.

### A. Video Object Segmentation

Video segmentation algorithms can be broadly categorized as unsupervised, semi-supervised and supervised methods, according to the level of supervision required.

Unsupervised algorithms do not require any manual annotation but usually rely on certain assumptions about the application scenario. Some techniques [4], [6], [7] emphasize the importance of motion information. More specially, [4], [6] analyze long term motion information via trajectories, then solve the segmentation as a trajectory clustering problem. [8], [9] introduce saliency information as prior knowledge to infer the object. Recently, [10], [11], [12] generate object segments via ranking several object candidates.

Semi-supervised video segmentation, which also refers to *label propagation*, is usually achieved via propagating human annotation specified on one or a few key-frames into the entire video sequence [13], [14], [15], [16], [17], [18], [19]. Those methods generally rely on flow-based random field propagation model [20], use patch seams based propagation strategy [21], solve an energy optimization problem over graph model [22], or segment pixels on bilateral space [23].

Supervised methods [24], [25], [26] generally require detailed user interactions and iterative human corrections. These methods are able to attain high-quality results while suffer from time-consuming human supervision.

### B. Point Trajectory

Trajectories are generated through tracking points over frames. Point trajectories show advantages for representing long term motion information. Kanade-Lucas-Tomasi (KLT) [27] is the dominant sparse method and tracks a small amount of feature points on time axis. After that, optical flow based dense trajectories [3] shows improvement over sparse interest points tracking, which inspires a lot of follow-up works in motion object segmentation and action recognition. In particular, [5], [28] introduce dense trajectories for action detection, which gains promising results. [4], [6] address the problem of unsupervised video segmentation, in which case the problem also be described as *motion segmentation*. These methods usually track points via dense optical flow for generating trajectories, and perform segmentation via clustering trajectories.

However, these approaches handle trajectories in single or pairs, ignore the inner coherence in a group of similar trajectories. In this paper, we operate trajectories as united super-trajectory groups instead of individual entities, thus offering compact and atomic video representation and fully exploiting spatiotemporal relations among trajectories.

## III. SUPER-TRAJECTORY VIA GROUPING TRAJECTORIES

In this work, we propose a semi-unsupervised video segmentation approach using super-trajectories. We first introduce the proposed super-trajectory in this section and then we describe our segmentation approach in Sec. IV.

In Sec. III-A, we present our trajectory generation method based on a probabilistic model. Then, in Sec. III-B, we introduce our super-trajectory generation method using density peaks based clustering (DPC) algorithm [1].

### A. Trajectory Generation

Given a sequence of video frames  $I_{1:T} = \{I_1, \dots, I_T\}$  within time range  $[1, T]$ , each pixel point can be tracked to the next frame using optical flow. This tracking process can be executed frame-by-frame until reaching some termination conditions (*e.g.*, occlusion, incorrect motion estimates, *etc.*). Those tracked points are composed into a trajectory and a new tracker is initialized where prior tracker finished. Contrast to previous trajectory methods that design many hard thresholds [4], [5], [6] for detecting occlusion, or unreliable motion estimates, we build our trajectory generation on a more interpretable and reasonable probabilistic model.

Let  $\mathbf{w}$  denote a flow field indexed by pixel positions that returns a 2D flow vector at a given point. Via LDOF [29], we compute forward flow field  $\mathbf{w}_t$  from frame  $I_t$  to  $I_{t+1}$ , and the backward flow field  $\hat{\mathbf{w}}_t$  from  $I_t$  to  $I_{t-1}$ , and we can track pixel position  $\mathbf{x} = (x, y, t)$  to the next and previous frames. Tracked points of subsequent frames are concatenated to form a trajectory  $\tau$ :

$$\tau = \{\mathbf{x}_n\}_{n=1}^L = \{(x_n, y_n, t_n)\}_{n=1}^L, \quad t_n \in [1, T], \quad (1)$$

where  $L$  indicates the length of trajectory  $\tau$  and  $(x_n, y_n) = (x_{n-1}, y_{n-1}) + \mathbf{w}_{t_{n-1}}(x_{n-1}, y_{n-1})$ . We model point tracking process as first order Markov, and denote the probability that  $n$ -th point  $\mathbf{x}_n$  of trajectory  $\tau$  is correctly tracked from frame  $I_{t_1}$  as  $p(\mathbf{x}_n | I_{t_1:t_n})$ . The prediction model is defined by:

$$p(\mathbf{x}_n | I_{t_1:t_n}) = p(\mathbf{x}_n | \mathbf{x}_{n-1}) p(\mathbf{x}_{n-1} | I_{t_1:t_{n-1}}), \quad (2)$$

where  $p(\mathbf{x}_1 | I_{t_1}) = 1$  and  $p(\mathbf{x}_n | \mathbf{x}_{n-1})$  is formulated as:

$$p(\mathbf{x}_n | \mathbf{x}_{n-1}) = \exp\{-\mathcal{E}_{app} + \mathcal{E}_{occ}\}. \quad (3)$$

The energy functions  $\mathcal{E}$  penalize various potential tracking error. The former energy  $\mathcal{E}_{app}$  is expressed as:

$$\mathcal{E}_{app}(\mathbf{x}_n, \mathbf{x}_{n-1}) = \|I_{t_n}(x_n, y_n) - I_{t_{n-1}}(x_{n-1}, y_{n-1})\|, \quad (4)$$

which penalizes the appearance variations between corresponding points. The latter energy  $\mathcal{E}_{occ}$  is for penalizing occlusions using the consistency of the forward and backward flows:

$$\mathcal{E}_{occ}(\mathbf{x}_n, \mathbf{x}_{n-1}) = \frac{\|\hat{\mathbf{w}}_{t_n}(x_n, y_n) + \mathbf{w}_{t_{n-1}}(x_{n-1}, y_{n-1})\|}{\|\hat{\mathbf{w}}_{t_n}(x_n, y_n)\| + \|\mathbf{w}_{t_{n-1}}(x_{n-1}, y_{n-1})\|}. \quad (5)$$

As discussed in [3], when this consistency constraint is violated, occlusion or unreliable optical flow estimates easily occur. Note that we find the proposed tracking model works well but our model is not limited by above constraints. We stop tracking points when  $p(\mathbf{x}_n | I_{t_1:t_n}) < 0.5$ , and then we start a new tracker at  $\mathbf{x}_n$ . In our implements, we discard trajectories shorter than four frames.

## B. Super-Trajectory Generation

Previous research noticed the value of trajectory for representing long term motion information. We furthermore find that neighbouring trajectories have compact spatiotemporal relationships and exhibit similar natures in appearance and motion patterns. This motivates us operating trajectories as united groups, thus offering an effective and convenient representation of video.

The proposed super-trajectory is generated via clustering trajectories using a recently proposed clustering algorithm: density peaks based clustering (DPC). Before we introduce our super-trajectory generation method, we first provide the basic knowledge for DPC [1].

**Density Peaks based Clustering (DPC)** DPC [1] is proposed to cluster the data by finding of density peaks. It provides a unique solution of fast clustering based on the idea that cluster centers are characterized by a higher density than their neighbors and by a relatively large distance from points with higher densities. It offers a reasonable criterion for finding clustering centers.

Given the distances  $d_{ij}$  between data points, for each data point  $i$ , DPC calculates two quantities: local density  $\rho_i$  and its distance  $\delta_i$  from points of higher density. The local density  $\rho_i$  of data point  $i$  is defined as <sup>1</sup>:

$$\rho_i = \sum_j d_{ij}. \quad (6)$$

$\delta_i$  is measured by computing the minimum distance between the point  $i$  and any other point with higher density:

$$\delta_i = \min_{j: \rho_j > \rho_i} (d_{ij}). \quad (7)$$

For the point with highest density, it takes  $\delta_i = \max_j (d_{ij})$ .

Cluster centers are the points with high local density ( $\rho \uparrow$ ) and large distance ( $\delta \uparrow$ ) from other points with higher local density. The data points can be ranked via  $\gamma_i = \rho_i \delta_i$ , and the top ranking points are selected as centers. After successful declaration of cluster centers, each remaining data points is assigned to the cluster center as its nearest neighbor of higher density.

**Grouping Trajectories via DPC** With a trajectory  $\tau = \{(x_n, y_n, t_n)\}_n$  spans  $L$  frames, we define three features: spatial location ( $l_\tau$ ), color ( $c_\tau$ ), and velocity ( $v_\tau$ ), for describing  $\tau$ :

$$l_\tau = \frac{1}{L} \sum_{n=1}^L (x_n, y_n), \quad c_\tau = \frac{1}{L} \sum_{n=1}^L I_{t_n}(x_n, y_n), \quad (8)$$

$$v_\tau = \frac{1}{L} \sum_{n=1}^L \left( \frac{1}{\Delta t} (x_{n+\Delta t} - x_n, y_{n+\Delta t} - y_n) \right),$$

where we set  $\Delta t = 3$ . We test  $\Delta t = \{5, 7, 9\}$  and do not observe obvious effect on the results.

Between each pair of trajectories  $\tau_i$  and  $\tau_j$  that share some frames, we define their distance  $d_{ij}$  via measuring descriptor similarity:

$$d_{ij} = \sum_{f=\{l,c,v\}} \|f_{\tau_i} - f_{\tau_j}\|. \quad (9)$$

<sup>1</sup>Here we do not use a cut-off kernel or gaussian kernel adopted in [1], due to the small data amount.

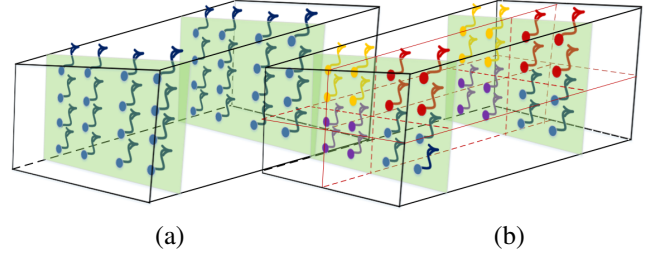


Fig. 2. Illustration of initial super-trajectory generation. (a) The arrows indicate trajectories and the dots indicate the initial location of trajectory. (b) We roughly divide all the trajectories into  $K$  groups with a given number of spatial grids  $K = 4$ .

If there is no any temporal overlap, we set  $d_{ij} = H$ , where  $H$  has a very large value.

The proposed super-trajectory method first roughly partitions trajectories into several non-overlap clusters, and then iteratively optimizes each partition to get the optimized trajectory clusters.

The only needed parameter of our super-trajectory algorithm is number of spatial grids  $K$ , as the degree of spatial subdivision. Then the spatial sampling step is  $R = \sqrt{S/K}$ , where  $S$  refers to the product of the height and width of image frame. The clustering procedure begins with an initialization step where we divide the input video  $I_{1:T}$  into several non-overlap spatiotemporal volumes of size  $R \times R \times T$ . As shown in Fig. 2, we further divide all trajectories  $\{\tau_i\}_i$  into those  $K$  volumes. A trajectory  $\tau$  falls into the volume where it starts. In this way, we roughly divide  $\{\tau_i\}_i$  into  $K$  spatially regular groups. Then we need to find a proper cluster number of each trajectory group, thereby further offering a reasonable temporal split of video.

We initially estimate the cluster number of each trajectory group as  $C = T/\bar{L}$ , where  $\bar{L}$  indicates the averaged length of all the trajectories. Then we apply a modified DPC algorithm for generating trajectory clusters, as described with in Alg. 1. In Alg. 1-3, if we have  $\delta_i = H$ , then trajectory  $\tau_i$  does not have any temporal overlap with those trajectories have higher local densities. That means trajectory  $\tau_i$  is the center of a

---

### Algorithm 1 DPC for Generating Super-Trajectory Centers

---

**Require:** A group of trajectories  $\{\tau_i\}_i$ , distance matrix  $\{d_{ij}\}$  via Eq. 9 and cluster number  $C$ ;

**Ensure:** Organized trajectory clusters;

- 1: Compute local densities  $\{\rho_i\}_i$  via Eq. 6;
  - 2: Compute distance  $\{\delta_i\}_i$  via Eq. 7;
  - 3: Find  $\{\tau_{i'}\}_{i'=1}^{n'}$  with  $\delta_{i'} = H$ ;
  - 4: **if**  $C < n'$  **then**
  - 5:   Select  $\{\tau_{i'}\}_{i'=1}^{n'}$  as cluster centers;
  - 6: **else**
  - 7:   Compute  $\{\gamma_i\}_i$  via  $\gamma_i = \rho_i \delta_i$ ;
  - 8:   Select the trajectories with  $C$  highest  $\gamma$  values as cluster centers;
  - 9: **end if**
  - 10: Assign remaining trajectories to cluster centers.
- 

isolated group. If  $C < n'$ , in Alg. 1-4, that means there exist



Fig. 3. Illustration of our super-trajectory generation via iterative trajectory clustering. (a) Frame  $I_t$ . (b)-(f) Visualization results of super-trajectory in time slice  $I_t$  with different iterations. Each point is assigned the averaged color of points of the super-trajectory which it belongs to. The blank areas are the discarded trajectories which are shorter than four frames.

more than  $C$  unconnected trajectory groups. Then we select the trajectories with highest densities of those unconnected trajectory groups as centers (Alg. 1-5). Otherwise, in Alg. 1-7,8, the trajectories with  $C$  highest  $\gamma$  values are selected as the cluster centers. The whole initialization process is described in Alg. 2-1,2,3.

Based on above initialization process, we roughly group trajectories into super-trajectories according to their spatiotemporal relationships and similarities (see Fig. 3(b)). Next, we iteratively refine our super-trajectory assignments. In this process, each trajectory is classified into the nearest cluster center. For reducing the searching space, we only search the trajectories fall into a  $2R \times 2R \times T$  space-time volume around the cluster center  $\tau_{i'}$  (Alg. 2-7). Once each trajectory has been associated to the nearest cluster center, an update step adjusts the center of each trajectory cluster via Alg. 1 with  $C = 1$  (Alg. 2-14,15). We drop very small trajectory clusters and combine those trajectories to other nearest trajectory clusters. In practice, we find 5 iterations for above refining process are enough for obtaining satisfactory performance. Visualization results of super-trajectory generation with different iterations are presented in Fig. 3.

Via Alg. 1, we group all trajectories  $\mathcal{T} = \{\tau_i\}_i$  into  $m$  nonoverlap clusters, represented as super-trajectories  $\mathcal{X} = \{\chi_j\}_{j=1}^m$ , where  $\chi_j = \{\tau_i | \tau_i \text{ is classified into } j\text{-th cluster via Alg. 2}\}$ . It is worth noting,  $m$ , the number of super-trajectories, is varied in each iteration in Alg. 2 since we merge small clusters into other clusters. Additionally,  $m$  for different videos is different even with same input parameter  $K$ . That is very important, since different videos have different temporal characteristics, thus we only constrain their spatial

shape via  $K$ .

---

#### Algorithm 2 Super-Trajectory Generation

---

**Require:** All the trajectories  $\{\tau_i\}_i$ , spatial sampling step  $R$ ;  
**Ensure:** Super-trajectory assignments;  
 /\* Initialization \*/  
 1: Obtain  $K$  trajectory groups via spatial sampling step  $R$ ;  
 2: Set initial cluster number  $C = T/\bar{L}$ ;  
 3: Obtain initial cluster centers  $\{\tau_{i'}\}_{i'}^m$  from each trajectory group via Alg. 1;  
 4: **loop**  
   /\* Iterative Assignment \*/  
 5: Set label  $l_i = -1$  and distance  $\kappa_i = H$  for each trajectory  $\tau_i$ ;  
 6: **for** each trajectory cluster center  $\tau_{i'}$  **do**  
 7:   **for** each trajectory  $\tau_j$  falls in a  $2R \times 2R \times T$  space-time volume around  $\tau_{i'}$  **do**  
 8:     Compute distance  $d_{ji'}$  between  $\tau_j$  and  $\tau_{i'}$  via Eq. 9;  
 9:     **if**  $d_{ji'} < \kappa_j$  **then**  
 10:       Set  $\kappa_j = d_{ji'}$ ,  $l_j = i'$ ;  
 11:     **end if**  
 12:   **end for**  
 13: **end for**  
   /\* Update Assignment \*/  
 14: Set cluster number  $C = 1$ ;  
 15: Update  $\{\tau_{i'}\}_{i'}^m$  from each cluster via Alg. 1.  
 16: **end loop**

---

#### IV. SUPER-TRAJECTORY BASED VIDEO SEGMENTATION

In Sec. III, we cluster a set of compact trajectories into super-trajectory. In this section, we describe our video segmentation approach that leverages the advantages of super-trajectory.

##### A. Super-Trajectory based Propagation

Given the mask  $\mathcal{M}$  of the first frame  $I_1$ , we seek a binary partitioning of pixels into foreground and background classes. Clearly, the annotation can be propagated to the rest of the video, using the trajectories that start at the first frame. However, only a few of points can be successfully tracked across the whole scene, due to occlusion, drift or unreliable motion estimation. Benefiting from our efficient trajectory clustering approach, super-trajectories are able to spread more annotation information over longer periods. This inspires us to base our label propagation process on super-trajectory.

For inferring the foreground probability of super-trajectories  $\mathcal{X}$ , we first divide all the trajectories  $\mathcal{T}$  into three categories: foreground trajectories  $\mathcal{T}^f$ , background trajectories  $\mathcal{T}^b$  and unlabeled trajectories  $\mathcal{T}^u$ , where  $\mathcal{T} = \mathcal{T}^f \cup \mathcal{T}^b \cup \mathcal{T}^u$ . The  $\mathcal{T}^f$  and  $\mathcal{T}^b$  are the trajectories which start at the first frame and are labeled by the annotation mask  $\mathcal{M}$ , while the  $\mathcal{T}^u$  are the trajectories start at any frames except the first frame, thus cannot be labeled via  $\mathcal{M}$ . Accordingly, super-trajectories  $\mathcal{X}$  are classified into two categories: labeled ones  $\mathcal{X}^l$  and unlabeled ones  $\mathcal{X}^u$ . A labeled super-trajectory  $\chi_j^l \in \mathcal{X}^l$  contains at least

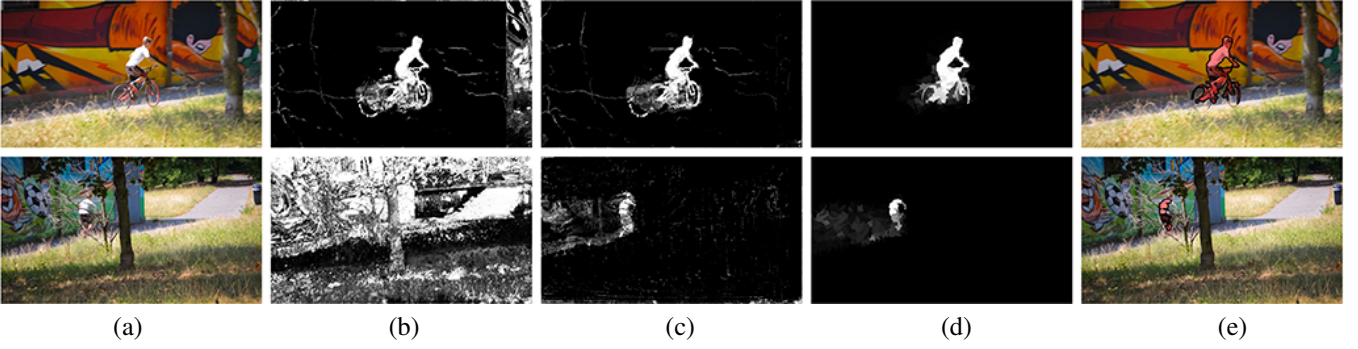


Fig. 4. (a) Input frames. (b) Foreground estimates via Eq. 10 and the appearance model in Sec. IV-A. (c) Foreground estimates via our reverse tracking strategy (Eq. 12) and the updated appearance model in Sec. IV-B. (d) Foreground estimates via backward re-occurrence based optimization (Eq. 14). (e) Final segmentation results.

one labeled trajectory from  $\mathcal{T}^f$  or  $\mathcal{T}^b$ , and its foreground probability can be computed as the ratio between the included foreground trajectories and the labeled ones it contains:

$$f(\chi_j^l) = \frac{|\chi_j^l \cap \mathcal{T}^f|}{|\chi_j^l \cap \mathcal{T}^f| + |\chi_j^l \cap \mathcal{T}^b|}. \quad (10)$$

For the points belonging to the labeled super-trajectory  $\chi_j^l$ , their foreground probabilities are set as  $f(\chi_j^l)$ .

Then we build an appearance model for estimating the foreground probabilities of unlabeled pixels. The appearance model is built upon the labeled super-trajectories  $\mathcal{X}^l$ , consists of two weighted Gaussian Mixture Models over RGB colour values, one for the foreground and one for the background. The foreground GMM is estimated from all labeled super-trajectories  $\mathcal{X}^l$ , weighted by their foreground probabilities  $\{f(\chi_j^l)\}$ . The estimation of background GMM is analogous, with the weight replaced by the background probabilities  $\{1 - f(\chi_j^l)\}$ . Since the labeled super-trajectories covers more content of videos, the corresponding appearance model is more accurate than the ones estimated from  $\mathcal{M}$  or labeled trajectories.

### B. Reverse Tracking

Although above model successfully propagates more annotation information across the whole video sequence, it still suffers from some difficulties: the model will be confused when a new object come into view (see Fig. 4 (b)). To this, we propose to *reverse track points* for excluding new incoming objects. We compute the ‘source’ of unlabeled trajectory  $\tau_i^u \in \mathcal{T}^u$ :

$$(x_0, y_0) = (x_1, y_1) - v_{\tau_i^u}, \quad (11)$$

where  $(x_1, y_1)$  indicates starting position and  $v_{\tau_i^u}$  refers to velocity via Eq. 8. It is clear that, if the virtual position  $(x_0, y_0)$  is out of image frame domain, trajectory  $\tau_i^u$  is a latecomer. For those trajectories  $\mathcal{T}^o \subset \mathcal{T}^u$  start outside view, we treat them as background. Labeled super-trajectory  $\chi_j^l \in \mathcal{X}^l$  is redefined as the one contains at least one trajectory from  $\mathcal{T}^f$ ,  $\mathcal{T}^b$  or  $\mathcal{T}^o$ , and Eq. 10 is updated as

$$f(\chi_j^l) = \frac{|\chi_j^l \cap \mathcal{T}^f|}{|\chi_j^l \cap \mathcal{T}^f| + |\chi_j^l \cap \mathcal{T}^b| + |\chi_j^l \cap \mathcal{T}^o|}. \quad (12)$$

Those outside trajectories  $\mathcal{T}^o$  are also adopted for training appearance model in prior step. According to our experiment in Sec. V, this assumption offers about 6% performance improvement. Foreground estimation results via our reverse tracking strategy are presented in Fig. 4 (c).

### C. Backward Re-Occurrence

For re-identifying objects after long-term occlusions and constraining segmentation consistency, we explore *re-occurrence* of objects. As suggested by [8], objects, or regions, often re-occur both in space and in time. Here, we build correspondences among re-occurring regions across distant frames and transport foreground estimates globally. This process is based on super-pixel level, since super-trajectories cannot cover all of pixels.

Let  $R_t = \{r_i^t\}_i$  be the superpixel set of frame  $I_t$ . For each region, we search its  $N$  Nearest Neighbors (NNs) as its re-occurring regions using KD-tree search. For region  $r_i^t$  of frame  $I_t$ , we only search its NNs in previous frames  $\{I_1, \dots, I_t\}$ . Such *backward search* strategy is for biasing the segmentation results of prior frames as the propagation accuracy degrades over time. Following [8], each region  $r_i$  is represented as a concatenation of several descriptors  $f_{r_i}$ : RGB and LAB color histograms (6 channels  $\times$  20 bins), HOG descriptor (9 cells  $\times$  6 orientation bins) computed over a  $15 \times 15$  patch around superpixel center, and spatial coordinate of superpixel center. The spatial coordinate is with respect to image center and normalized into  $[0, 1]$ , which implicitly incorporates spatial consistency in NN-search.

After NN-search in the feature space, we construct a weight matrix  $W$  for all the regions  $\{R_t\}_t = \{r_i\}_i$ :

$$W_{ij} = \begin{cases} e^{-\|f_{r_i} - f_{r_j}\|} & \text{if } r_j \text{ is one of NNs of } r_i \\ 1 & \text{if } i = j \\ 0 & \text{otherwise} \end{cases} \quad (13)$$

Then a probability transition matrix  $P$  is built via row-wise normalization of  $W$ . We define a column vector  $v$  that gathers all the foreground probabilities of  $\{r_i\}_i$ . The foreground probability of a superpixel is assigned as the average foreground probabilities of its pixels.

Video	IoU score $\mathcal{J}$							Contour Accuracy $\mathcal{F}$						
	BVS	FCP	JMP	SEA	TSP	HVS	STV	BVS	FCP	JMP	SEA	TSP	HVS	STV
breakdance-flare	0.727	0.723	0.430	0.131	0.040	0.499	<b>0.834</b>	0.689	0.738	0.523	0.167	0.116	0.625	<b>0.890</b>
camel	0.669	0.734	0.640	0.649	0.654	<b>0.876</b>	0.795	0.645	0.617	0.711	0.614	0.529	<b>0.871</b>	0.787
car-roundabout	0.851	0.717	0.726	0.708	0.614	0.777	<b>0.907</b>	0.407	0.478	0.619	0.710	0.435	0.551	<b>0.829</b>
dance-twirl	0.492	0.471	0.444	0.117	0.099	0.318	<b>0.618</b>	<b>0.602</b>	0.427	0.520	0.213	0.128	0.516	0.595
drift-chicane	0.033	<b>0.457</b>	0.243	0.119	0.018	0.331	0.441	<b>0.764</b>	0.477	0.338	0.159	0.033	0.547	0.563
horsejump-low	0.601	0.607	0.663	0.498	0.291	0.551	<b>0.763</b>	0.594	0.533	0.696	0.548	0.356	0.572	<b>0.781</b>
libby	<b>0.776</b>	0.316	0.295	0.226	0.070	0.553	0.728	0.790	0.389	0.365	0.209	0.091	0.641	<b>0.807</b>
mallard-fly	0.606	0.541	0.536	0.557	0.200	0.436	<b>0.651</b>	0.346	0.539	0.579	0.607	0.235	0.441	<b>0.716</b>
motorbike	0.563	0.713	0.506	0.451	0.340	0.687	<b>0.738</b>	<b>0.844</b>	0.632	0.578	0.481	0.406	0.823	0.770
rhino	0.782	0.794	0.716	0.736	0.694	0.812	<b>0.894</b>	0.746	0.647	0.653	0.658	0.499	0.658	<b>0.815</b>
soapbox	<b>0.789</b>	0.449	0.759	0.783	0.247	0.684	0.744	0.678	0.423	0.677	<b>0.750</b>	0.336	0.690	0.714
stroller	0.767	0.597	0.656	0.464	0.369	0.662	<b>0.826</b>	0.624	0.581	0.718	0.525	0.404	0.708	<b>0.870</b>
surf	0.492	0.843	<b>0.941</b>	0.821	0.814	0.759	0.917	0.371	0.713	<b>0.872</b>	0.732	0.641	0.652	0.868
swing	<b>0.784</b>	0.648	0.115	0.511	0.098	0.104	0.759	<b>0.839</b>	0.538	0.109	0.409	0.087	0.091	0.687
tennis	0.737	0.623	0.765	0.482	0.074	0.576	<b>0.829</b>	0.590	0.652	0.818	0.537	0.114	0.579	<b>0.898</b>
Avg.	0.665	0.631	0.607	0.556	0.358	0.596	<b>0.736</b>	0.656	0.546	0.586	0.533	0.346	0.576	<b>0.720</b>

TABLE I

IOU SCORE ( $\mathcal{J}$ ) AND CONTOUR ACCURACY ( $\mathcal{F}$ ) ON A REPRESENTATIVE SUBSET OF THE DAVIS DATASET [2], AND THE AVERAGE COMPUTED OVER ALL 50 VIDEO SEQUENCES. FOR BOTH TWO MEASURE METRICS, HIGHER VALUES ARE BETTER. THE BEST RESULTS ARE BOLDFACED.

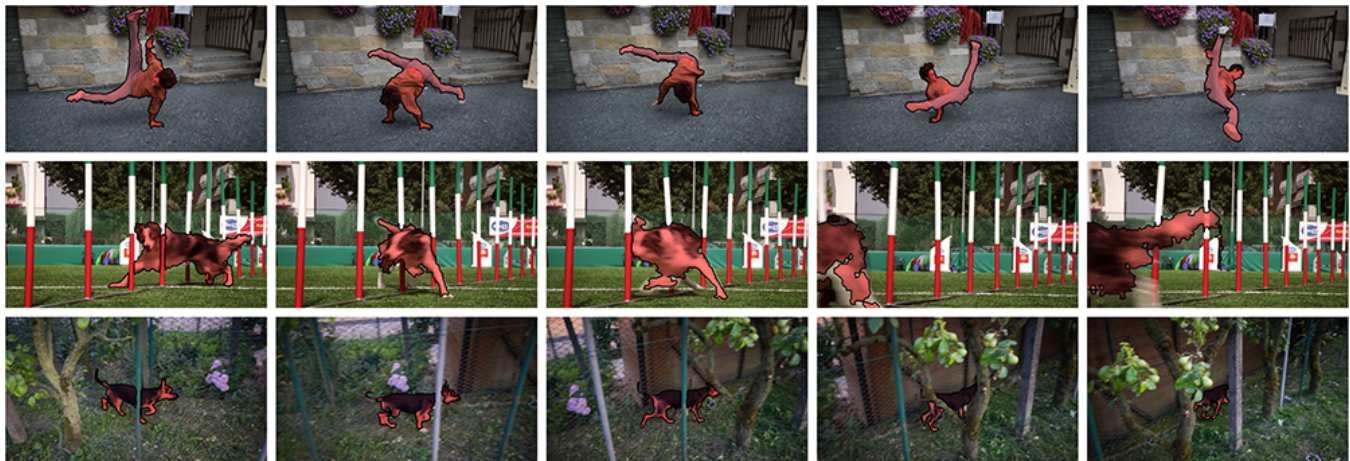


Fig. 5. Qualitative segmentation results on three video sequences from DAVIS [2] (from top to bottom: *breakdance-flare*, *dog-agility* and *libby*). It can be observed that the proposed algorithm is applicable to a quite general set of sequences and robust to many challenges.

Then we iteratively update  $v$  via the probability transition matrix  $P$ . In each iteration  $k$ , we update  $v^{(k)}$  via:

$$v^{(k)} = P v^{(k-1)}, \quad (14)$$

which equivalent to updating foreground probability of a region with the weighted average of its NNs. In each iteration, we keep the foreground probabilities of those points belonging to labeled trajectories unchanged. Then we recompute  $v^{(k)}$  and update it in next iteration. In this way, the relatively accurate annotation information of the labeled trajectories is preserved. Additionally, the annotation information is progressively propagated in a forward way and the super-trajectories based foreground estimates are consistent even across many distant frames (see Fig. 4 (d)).

After 10 iterations, the pixels (regions) with foreground probabilities larger than 0.5 are classified as foreground, thus obtaining final binary segments. In Sec. V, we test  $N = \{4, 6, \dots, 20\}$  and only observe  $\pm 0.3\%$  performance variation. We set  $N = 8$  for obtaining best performance.

## V. EXPERIMENTAL RESULTS

**Parameter Settings** In Sec. III-B, we set number of spatial grids  $K = 1200$ . In Sec. IV-C, we over-segment each frame into about 2000 superpixels via SLIC [30] for well boundary adherence. For each superpixel, we set the number of NNs  $N = 8$ . In our experiments, all the parameters of our algorithm are fixed to unity.

**Datasets** We evaluate our method on new released DAVIS dataset [2]. DAVIS dataset contains 50 video sequences and pixel-level manual ground-truth for the foreground object in every frame. Those videos span a wide range of object segmentation challenges such as occlusions, fast-motion and appearance changes. Since DAVIS contains diverse scenarios which break classical assumptions, as demonstrated in [2], most state-of-the-art methods fail to produce reasonable segments.

### A. Performance Comparison

To evaluate the quality of the proposed super-trajectory based video segmentation (STV), we provide in this section

both qualitative as well as quantitative comparison on DAVIS dataset [2].

Two measures offered in DAVIS dataset are employed for the quantitative evaluation: intersection-over-union score ( $\mathcal{J}$ ) and contour accuracy ( $\mathcal{F}$ ). Given a segmentation mask  $M$  and ground-truth  $G$ , intersection-over-union score is defined as  $\mathcal{J} = \frac{M \cap G}{M \cup G}$ . Contour accuracy ( $\mathcal{F}$ ) is for measuring how well the segment contours  $c(M)$  match the ground-truth contour  $c(G)$ . Contour-based precision  $P_c$  and recall  $R_c$  between  $c(M)$  and  $c(G)$  can be computed via bipartite graph matching. Given  $P_c$  and  $R_c$ , contour accuracy  $\mathcal{F}$  is defined as  $\mathcal{F} = \frac{2P_c R_c}{P_c + R_c}$ .

In Table 1, we report IoU score ( $\mathcal{J}$ ) and contour accuracy ( $\mathcal{F}$ ) on a representative subset of the DAVIS dataset. All the matrixes are averaged across video sequences. We compare the proposed STV against six top-performing alternatives: BVS [23], FCP [22], JMP [26], SEA [21], TSP [31] and HVS [32]. As shown, the proposed STV performs superior on most video sequences. And STV achieves the highest average IoU score (**0.736**) over all the 50 video sequence of the DAVIS dataset, which demonstrates significant improvement over the second best algorithm BVS (0.665), and third best algorithm FCP (0.631). In addition, STV achieves the best overall contour accuracy (**0.720**) over other algorithms. This demonstrates that our segments align better with the ground-truth object boundaries.

Qualitative video segmentation results for three video sequences from the DAVIS dataset [2] are presented in Fig 5. With the first frame as initialization, the proposed algorithm has the ability to segment the objects with fast motion patterns (*breakdance-flare*) or large shape deformation (*dog-agility*). It also produces accurate segmentation maps even when the foreground suffers occlusions (*libby*).

### B. Validation of the Proposed Algorithm

In this section, we offer more detailed exploration for the proposed approach in several aspects. We test the values of important parameters, verify basic assumptions of the proposed algorithm, and evaluate the contributions from each part of our approach.

We first study the influence of the needed input parameter: number of spatial grids  $K$ , of our super-trajectory algorithm in Sec. III-B. We report the performance by plotting the IoU value ( $\mathcal{J}$ ) of the segmentation results as functions of a variety of  $K$ s, where we vary  $K = \{800, 900, \dots, 1500\}$ . As shown in Fig. 6 (a), the performance increases with finer super-trajectory clustering in spatial domain ( $K \uparrow$ ). However, when we further increase  $K$ , the final performance does not change obviously. We set  $K = 1200$  where the maximum performance is obtained. Later, we investigate the influence of parameter  $N$ , which indicates the number of the NNs of a region in Sec. IV-C. We plot IoU score ( $\mathcal{J}$ ) with varying  $N = \{2, 4, \dots, 20\}$  in Fig. 6 (b), and set  $N = 8$  for achieving best performance.

To quantify the improvement obtained with our proposed trajectories in Sec. III-A, we compare to two baseline trajectories: DTM [6] and DAD [5] in our experimental results. DTM is widely used for motion segmentation and DAD shows

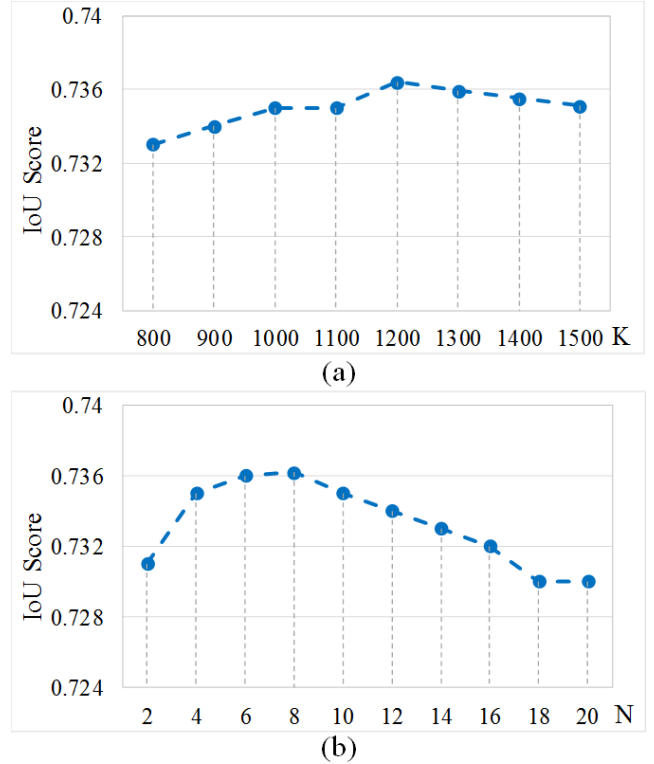


Fig. 6. Parameter selection for number of spatial grids  $K$  (a) and the number of the NNs  $N$  (b). The IoU score is plotted as a function of a variety of  $K$ s ( $N$ s).

	IoU score $\mathcal{J}$	Contour Accuracy $\mathcal{F}$
DTM	0.718	0.704
DAD	0.654	0.634
STV-s	0.605	0.587
STV-r	0.678	0.678
STV-b	0.696	0.683
STV	0.736	0.720

TABLE II  
AVERAGE IOU SCORE  $\mathcal{J}$  AND CONTOUR ACCURACY  $\mathcal{F}$  FOR THE DAVIS DATASET [2]. WE COMPARE OUR STV WITH TWO CLASSICAL TRAJECTORY METHODS [6], [5], AND THREE VARIATIONS OF OUR ALGORITHM.

promising performance for action detection. To be fair, we only replace our trajectory generation part with above two methods, estimate optical flow via LDOF [29] and keep all other parameters fixed.

To further dissect various parts of our method, we offer three variations of the proposed algorithm STV. For demonstrating the effectiveness of the our super-trajectory based label propagation in Sec. IV-A, we offer a baseline STV-s: perform label propagation on trajectory level and only use labeled-trajectories for establishing appearance model. For evaluating the effectiveness of the proposed reverse tracking strategy in Sec. IV-B, we offer a baseline STV-r: perform segmentation without considering outside trajectories  $\mathcal{T}^o$ . For evaluating the effectiveness of the background re-occurrence assumption, we offer a baseline STV-b: perform segmentation without Eq.14.

The comparison results with above baselines are summarized in Table 2. Three important conclusions can be drawn: (1) compared with classical trajectory methods [6], [5], the

proposed trajectory generation approach is preferable; (2) significant improvement over STV-s (0.736 *vs* 0.605) clearly demonstrates the advantage of super-trajectory for capturing rich structure information of video; (3) the improvement over STV-r and STV-b verifies the effectiveness of our reverse tracking strategy and global optimization via backward re-occurrence.

## VI. CONCLUSIONS

This paper introduced a video segmentation approach by representing video as super-trajectories. Based on DPC algorithm, compact trajectories are efficiently grouped into super-trajectories. Occlusion and drift are naturally handled by our trajectory generation method based on a probabilistic model. We proposed to perform video segmentation on super-trajectory level. Via reverse tracking points and leveraging the property of region re-occurrence, the algorithm is robust for many segmentation challenges. Experimental results demonstrate that our approach outperforms current state-of-the-art methods.

## REFERENCES

- [1] A. Rodriguez and A. Laio, "Clustering by fast search and find of density peaks," *Science*, 2014.
- [2] F. Perazzi, J. Pont-Tuset, B. McWilliams, L. V. Gool, M. Gross, and A. Sorkine-Hornung, "A benchmark dataset and evaluation methodology for video object segmentation," in *CVPR*, 2016.
- [3] N. Sundaram, T. Brox, and K. Keutzer, "Dense point trajectories by gpu-accelerated large displacement optical flow," in *ECCV*, 2010.
- [4] T. Brox and J. Malik, "Object segmentation by long term analysis of point trajectories," in *ECCV*, 2010.
- [5] H. Wang, A. Kläser, C. Schmid, and C.-L. Liu, "Action recognition by dense trajectories," in *CVPR*, 2011.
- [6] K. Fragkiadaki, G. Zhang, and J. Shi, "Video segmentation by tracing discontinuities in a trajectory embedding," in *CVPR*, 2012.
- [7] A. Papazoglou and V. Ferrari, "Fast object segmentation in unconstrained video," in *ICCV*, 2013.
- [8] A. Faktor and M. Irani, "Video segmentation by non-local consensus voting," in *BMVC*, 2014.
- [9] W. Wang, J. Shen, and F. Porikli, "Saliency-aware geodesic video object segmentation," in *CVPR*, 2015.
- [10] Y. J. Lee, J. Kim, and K. Grauman, "Key-segments for video object segmentation," in *ICCV*, 2011.
- [11] T. Ma and L. J. Latecki, "Maximum weight cliques with mutex constraints for video object segmentation," in *CVPR*, 2012.
- [12] D. Zhang, O. Javed, and M. Shah, "Video object segmentation through spatially accurate and temporally dense extraction of primary object regions," in *CVPR*, 2013.
- [13] W. Brendel and S. Todorovic, "Video object segmentation by tracking regions," in *ICCV*, 2009.
- [14] V. Badrinarayanan, F. Galasso, and R. Cipolla, "Label propagation in video sequences," in *CVPR*, 2010.
- [15] D. Tsai, M. Flagg, and J. M. Rehg, "Motion coherent tracking using multi-label MRF optimization," *BMVC*, 2010.
- [16] I. Budvytis, V. Badrinarayanan, and R. Cipolla, "Semi-supervised video segmentation using tree structured graphical models," in *CVPR*, 2011.
- [17] F. Li, T. Kim, A. Humayun, D. Tsai, and J. M. Rehg, "Video segmentation by tracking many figure-ground segments," in *ICCV*, 2013.
- [18] N. Shankar Nagaraja, F. R. Schmidt, and T. Brox, "Video segmentation with just a few strokes," in *ICCV*, 2015.
- [19] Y.-H. Tsai, M.-H. Yang, and M. J. Black, "Video segmentation via object flow," in *CVPR*, 2016.
- [20] S. Vijayanarasimhan and K. Grauman, "Active frame selection for label propagation in videos," in *ECCV*, 2012.
- [21] S. A. Ramakanth and R. V. Babu, "Seamseg: Video object segmentation using patch seams," in *CVPR*, 2014.
- [22] F. Perazzi, O. Wang, M. Gross, and A. Sorkinehornung, "Fully connected object proposals for video segmentation," in *CVPR*, 2015.
- [23] N. Maerki, F. Perazzi, O. Wang, and A. Sorkine-Hornung, "Bilateral space video segmentation," in *CVPR*, 2016.
- [24] X. Bai, J. Wang, D. Simons, and G. Sapiro, "Video snapcut: robust video object cutout using localized classifiers," *ACM Trans. on Graphics*, 2009.
- [25] A. Criminisi, T. Sharp, C. Rother, and P. P'Erez, "Geodesic image and video editing," *ACM Trans. on Graphics*, 2010.
- [26] Q. Fan, F. Zhong, D. Lischinski, D. Cohen-Or, and B. Chen, "Jumpcut: non-successive mask transfer and interpolation for video cutout," *ACM Trans. on Graphics*, 2015.
- [27] J. Shi and C. Tomasi, "Good features to track," in *CVPR*, 1994.
- [28] H. Wang and C. Schmid, "Action recognition with improved trajectories," in *ICCV*, 2013.
- [29] T. Brox and J. Malik, "Large displacement optical flow: Descriptor matching in variational motion estimation," *IEEE PAMI*, 2011.
- [30] R. Achanta, A. Shaji, K. Smith, A. Lucchi, P. Fua, and S. Susstrunk, "SLIC superpixels compared to state-of-the-art superpixel methods," *IEEE PAMI*, 2012.
- [31] J. Chang, D. Wei, and J. W. Fisher, "A video representation using temporal superpixels," in *CVPR*, 2013.
- [32] M. Grundmann, V. Kwatra, M. Han, and I. Essa, "Efficient hierarchical graph-based video segmentation," in *CVPR*, 2010.